Tribol Lett (2016) 64:23
DOI 10.1007/s11249-016-0756-x

ORIGINAL PAPER

Effect of a Fatty Acid Additive on the Kinetic Friction and Stiction of Confined Liquid Lubricants

Shinji Yamada[1,4] · Kyeong A Inomata[1] · Eriko Kobayashi[1] · Tadao Tanabe[1] · Kazue Kurihara[2,3]

Received: 26 June 2016 / Accepted: 12 September 2016 / Published online: 27 September 2016

Abstract The kinetic friction and stiction properties of the dilute solution of palmitic acid (PA, friction modifier additive) in poly(α-olefin) (PAO) confined between molecularly smooth mica surfaces were investigated using the surface forces apparatus (SFA). The results were contrasted with those of confined PAO system; the effects of PA additive on the confined film structure and friction/stiction properties were discussed. The hard-wall thickness of the PA/PAO system was 4.2 ± 0.1 nm, and that of the PAO system was below 1.4 nm. Considering the molecular size, the PA/PAO system has a monomolecular layer of PAO confined between PA adsorbed monolayers on mica surfaces. The kinetic friction of the PA/PAO system decreased with the increase of sliding velocity V, whereas the kinetic friction of the PAO system increased with the increase of V. The stiction spike height of the PA/PAO system increased with the increase of applied load L (pressure P), whereas the spike height of the PAO system decreased with the increase of L (P). These results imply totally different confined structures/sliding mechanisms for the two systems: solid-like slippage of PAO monomolecular layer between PA adsorbed monolayers for the PA/PAO system; and the extreme viscosity increase of PAO and resulting glass-like transition for the PAO system. The kinetic friction and stiction were larger for the PA/PAO system, which comes from the extreme confinement of PAO (only monomolecular layer) and strong van der Waals adhesion between the solid-like interfaces. The SFA results for smooth surfaces obtained here seem inconsistent with the observations in macroscopic tribology; palmitic acid dissolved in PAO reduces kinetic friction and stiction of engineering (rough) surfaces. The discrepancy of the friction behaviors between smooth and rough surfaces is discussed, which gives insights into designing low-friction surfaces in the oil-based lubrication of macroscopic tribology.

Keywords Nanotribology · Confined liquid lubricant · Friction modifier additive · Surface forces apparatus

1 Introduction

Reducing friction is one of the most important requirements for improving the performance of moving components and saving energy in many practical applications of mechanical systems. For this purpose, low-viscosity lubricant oils are commonly used to obtain low friction at high sliding velocity/low applied load conditions (hydrodynamic lubrication regime). However, such low-viscosity

Electronic supplementary material The online version of this article (doi:10.1007/s11249-016-0756-x) contains supplementary material, which is available to authorized users.

✉ Shinji Yamada
yamada.s@kao.co.jp

✉ Kazue Kurihara
kurihara@tagen.tohoku.ac.jp

[1] New Industry Creation Hatchery Center, Tohoku University, 6-6-10 Aoba, Aramaki, Aoba-ku, Sendai, Miyagi 980-8579, Japan

[2] Institute of Multidisciplinary Research for Advanced Materials, Tohoku University, 2-1-1 Katahira, Aoba-ku, Sendai, Miyagi 980-8577, Japan

[3] Advanced Institute for Materials Research, Tohoku University, 2-1-1 Katahira, Aoba-ku, Sendai, Miyagi 980-8577, Japan

[4] Present Address: Analytical Science Research Laboratories, Kao Corporation, 1334 Minato, Wakayama, Wakayama 640-8580, Japan

lubricant oils are easily squeezed out from the contact interfaces at low sliding velocity/high applied load conditions (boundary lubrication regime). Recent fundamental researches (both experiments and computer simulations) on the dynamics of confined simple lubricant liquids revealed that at least a few layers of liquid molecules could remain at the solid/solid contact interface even under extremely large normal pressure [1–4]. The intervening liquid molecules tend to pack into structures in confinement and often exhibit an extreme increase in viscosity and/or solid-like shear responses such as stiction and stick–slip sliding [1–7], which results in the large friction in boundary lubrication.

One of the approaches to reduce friction in boundary lubrication regime using low-viscosity lubricant oils is to add friction modifiers [8], and fatty acids (FAs) are the representative examples [9–12]. The FA molecules dissolved in lubricant base oils form an adsorbed monolayer on solid surface and increase the lubricant thickness at the contact interface, which contributes to load-bearing capability and low friction. In this study, particular attention is focused on saturated FA additives.

The interfacial structures and friction mechanisms of FA/base oil systems at the molecular level have been studied experimentally and theoretically by a number of authors. With regard to experiments, the surface forces apparatus (SFA) equipped with sliding attachments is effectively used because of its potential to measure the lubricant film thickness and contact area accurately during sliding [13, 14]. The well-defined contact geometry of the SFA is suitable to compare the experimental results with computer simulations [4]; this is another advantage of using the SFA for friction studies.

Ruths et al. [9] investigated the film structure and shear properties of the dilute solution of palmitic acid (PA) in tetradecane (model base oil) confined between mica surfaces by the SFA nanorheological measurement. Newtonian-like linear relationship between shear stress and shear rate was observed at low shear rate, and non-Newtonian behavior was observed at higher shear rate. They proposed a structural model that loose-packed PA monolayers are formed on opposed mica surfaces and hexadecane molecules are confined between them; some hexadecane molecules penetrate into the adsorbed PA monolayers. The rather disordered interfacial structure of the PA/tetradecane system induces liquid-like shear properties at low shear rate, which contributes to suppress static friction (stiction) and friction-induced vibrations in practical (macroscopic rough) surface systems.

Lundgren et al. [10] studied the friction properties of the dilute solution of stearic acid (SA) in *n*-hexadecane using the SFA. They obtained the friction coefficient μ of about 0.055 for the system, which was lower than that of pure *n*-hexadecane (μ of about 0.11). They speculated an interfacial structure that loose-packed SA monolayers are formed on opposed mica surfaces and about 1-nm thick of *n*-hexadecane layer is confined between them; *n*-hexadecane molecules penetrate into the adsorbed SA monolayers. The low friction of the system is again interpreted by the disordered structure of the confined film.

In this study, SFA friction measurements were taken for the dilute solution of palmitic acid (PA) in poly(α-olefin) (PAO). PAO is a commercial lubricant base oil used in many industrial applications, and additive solubility in PAO is generally lower than that in hydrocarbon oils [15]. The interfacial structure and resulting friction properties of FA additive/base oil systems should be dependent on the additive solubility in the system, which is our motivation of this study. Kinetic friction measurement was made as a function of applied load and sliding velocity, and stop-start stiction measurement was made as a function of applied load and surface stopping (aging) time. The results were contrasted with those of confined PAO system, and the effects of PA additive on the confined film structure and friction/stiction properties were discussed. The confined hard-wall thickness indicated the formation of adsorbed PA monolayers on opposed mica surfaces and a monomolecular layer of PAO was trapped between them. The observed friction behaviors (both kinetic friction and stiction) imply a slippage of the PAO monomolecular layer between the PA adsorbed monolayers; the confined system constitutes a solid-like contact interface, and no penetration of PAO molecules into the PA monolayers is expected. Our results show that the solid-like interface introduced by the PA adsorbed monolayers is effective to reduce kinetic friction and stiction between macroscopic rough surfaces in oil-based lubrication.

2 Experimental Section

The lubricant base oil investigated in this study was poly(α-olefin) (PAO, hydrogenated oligomers of 1-decene, industrial grade). The bulk viscosity of the PAO was 76 mPa s. Palmitic acid (PA) was examined as an additive, which was purchased from Nacalai Tesque Inc. (Japan) and used as received. The PA additive was dissolved in PAO at the concentration of 0.1 wt% (henceforth: PA/PAO).

Friction properties of the two confined lubricant systems, PAO (without additive) and PA/PAO, were investigated using the surface forces apparatus RSM-1 (Advance Riko, Inc., Japan) [16] modified for sliding experiments. This SFA model uses twin-path method (two-beam interferometry technique) to measure surface distance, which is effective to study the interactions between non-transparent surfaces. However, the twin-path method measures the

change in surface distance and does not give the confined film thickness. In this study, we believed that the direct measurement of film thickness and real contact area was important to investigate the effect of PA additive on friction mechanisms. The RSM-1 apparatus can be used as a conventional SFA (measuring surface distance using fringes of equal chromatic order, FECO) by removing the twin-path unit from the main chamber. Therefore, we used mica as a substrate material and performed conventional FECO-SFA measurement using the RSM-1 apparatus. Two cylindrical mica surfaces were positioned in a crossed cylinder configuration and were used to confine lubricant samples. When the mica substrates were installed into the apparatus, some P_2O_5 was placed inside the sealed chamber to keep the internal atmosphere completely dry during friction measurement. A droplet of a lubricant sample (vol. $\sim$0.1 ml) was injected between the mica surfaces. When brought together under an external load L (pressure P), the surfaces became flat because of the elastic deformation of the glue layer under each mica surface and the confined lubricant formed a molecularly thin film (see Fig. 1). Friction measurements were taken using a home-built bimorph slider [17]. Lateral motion (reversible cycling) at a constant sliding velocity V (ranged from 0.0056 to 5.6 μm/s) was applied to the lower surface. The resulting friction force F was measured using the resonance shear unit of the RSM-1 [18]; the deflection of the friction-measuring springs (spring constant $k = 2140$ N/m) which support the upper surface was measured by a capacitance probe. The applied load L (in the range $\sim$40 mN) was controlled by a normal force spring of the bimorph slider (spring constant $k = 1810$ N/m). Using multiple beam interferometry (MBI) [19], a cross-sectional image of the contact area (contact geometry) can be continuously monitored during sliding. Fringes of equal chromatic order (FECO) are obtained by passing a beam of white light normally through the substrate surfaces, which allows the measurement of the film thickness D (accuracy of 0.1 nm) and the size of the contact area A in real time. We should note that there is a contact pressure distribution within the contact area (maximum at the center) that could affect local molecular mobility; the confined liquid structures and friction/stiction properties discussed in this paper describe the average properties of the film. The experimental room was kept at a fixed temperature of 23 $\pm$ 1 °C.

3 Results

3.1 Hard-Wall and Dynamic Thickness

When a droplet of PAO was confined between two mica surfaces by normal compression, two distinct static hard-wall thicknesses (compressed film thickness at which the repulsive surface force (steric force of trapped liquid molecules) diverges), $D = 1.1 \pm 0.1$ nm and 1.4 ± 0.1 nm, were obtained at different contact positions (different measurements) [20]. This is probably due to the different confinement rates (surface approach rates) between different measurements [21]. For the PA/PAO system, the hard-wall thickness was 4.2 ± 0.1 nm. The thickness during sliding and that at the stop/start events were the same as the static hard-wall thickness for the two systems in our whole experiments; no measureable thickness change was observed within the resolution of the FECO technique. In addition, increasing load did not decrease the dynamic thickness for the two systems.

3.2 Kinetic Friction

The kinetic friction force was measured as a function of sliding velocity for the two systems at different applied load conditions; the results are shown in Fig. 2. For the PAO system (Fig. 2a), results for the two different hard-

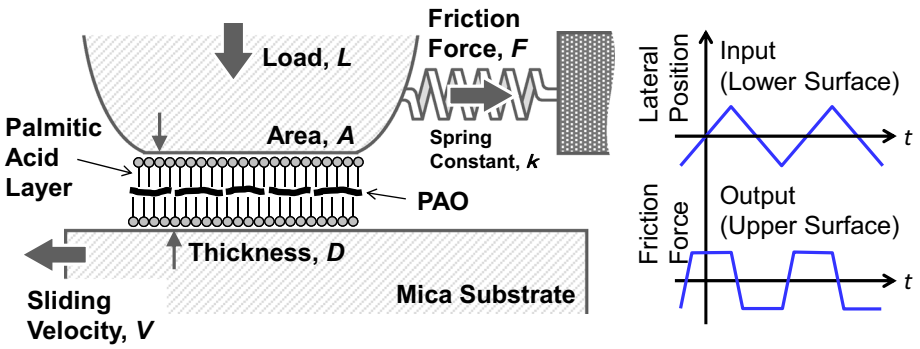

Fig. 1 Schematic drawing of the SFA friction measurement. The lubricant liquid was confined between molecularly smooth mica surfaces under an applied load L (pressure $P = L/A$). Lateral sliding motions at a constant velocity V were applied to the lower surface, and resulting friction force F was measured by a friction-measuring spring (spring constant k) that support the upper surface. The thickness of the film D and the real contact area A were measured from an optical technique using FECO fringes

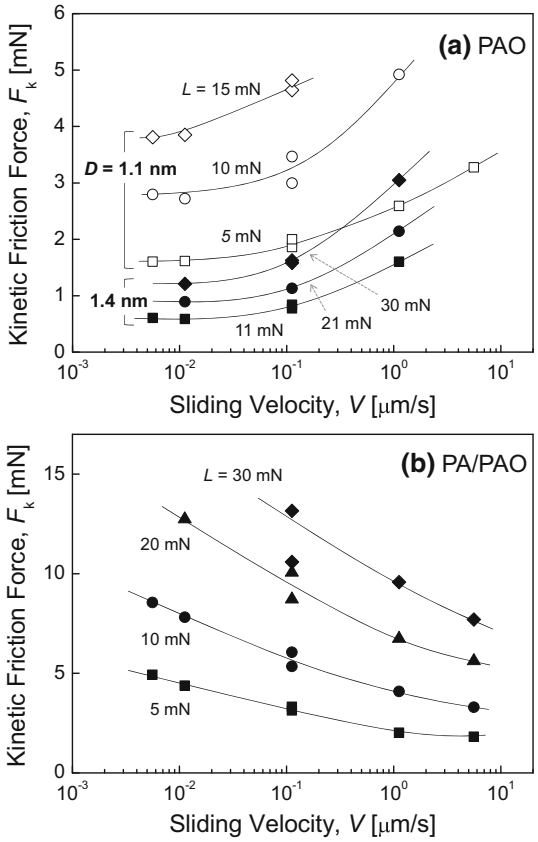

Fig. 2 Kinetic friction force as a function of sliding velocity at different applied load conditions; **a** confined PAO system, and **b** confined PA/PAO system. For the confined PAO system (**a**), two distinct hard-wall thicknesses ($D = 1.1$ and 1.4 nm) were obtained; the thinner film (*open symbols*) exhibited higher friction

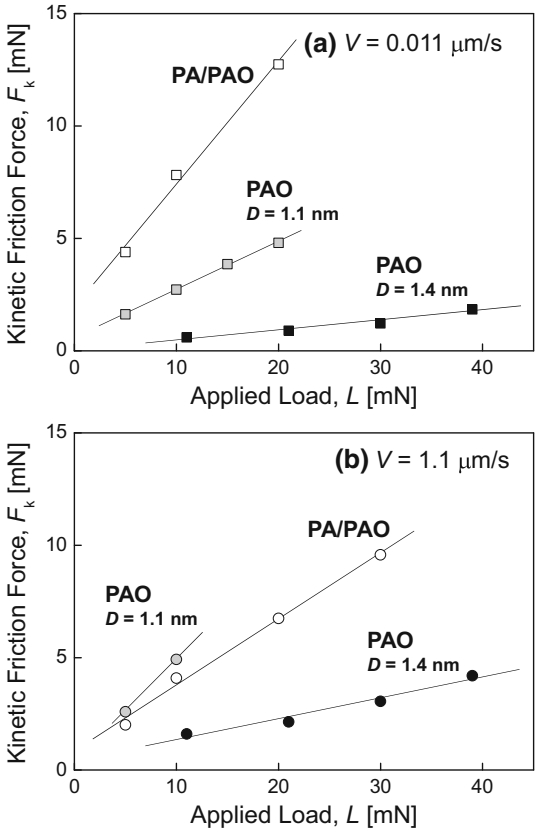

Fig. 3 Kinetic friction force as a function of applied load for the two confined systems at two different sliding velocities; **a** $V = 0.011$ μm/s, and **b** $V = 1.1$ μm/s. For the PAO system, results for the two distinct hard-wall thicknesses are plotted

wall thicknesses (1.4 nm and 1.1 nm) were plotted. Kinetic friction force was larger for the 1.1-nm film than the 1.4-nm film. For the both thickness films, kinetic friction force increased with the increase of applied load and sliding velocity. The PA/PAO system exhibited a different behavior (Fig. 2b). Kinetic friction force for the PA/PAO system was generally larger than that of the PAO system. The kinetic friction force increased with the increase of applied load, but decreased with the increase of sliding velocity.

Figure 3 shows the kinetic friction force F as a function of applied load L for the two confined systems at two different sliding velocities ($V = 0.011$ and 1.1 μm/s). The data were fitted by the "modified" Amontons' law considering the adhesion contribution on friction [1, 2]:

$$F = F_0 + \mu L \tag{1}$$

where F_0 is the zero-load friction (adhesion contribution) and μ is the friction coefficient. The two parameters obtained from the fit are listed in Table 1. Friction coefficient was the lowest for the 1.4-nm PAO film at the two sliding velocities. The addition of PA is not effective to reduce friction particularly at low sliding velocity; the friction coefficient of the confined PA/PAO films at $V = 0.011$ μm/s was 0.54, which was approximately an order of magnitude larger than the 1.4-nm PAO film. The zero-load friction was the largest for the PA/PAO system at both velocity conditions.

Table 1 Zero-load friction F_0 and friction coefficient μ for the two confined systems obtained for the results shown in Fig. 3 using Eq. 1

	$V = 0.011$ μm/s		$V = 1.1$ μm/s	
	F_0	μ	F_0	μ
PAO				
1.1 nm	0.58 ± 0.08	0.21 ± 0.01	0.26	0.47
1.4 nm	0.03 ± 0.18	0.04 ± 0.01	0.40 ± 0.33	0.09 ± 0.01
PA/PAO	1.93 ± 0.63	0.54 ± 0.05	0.81 ± 0.30	0.29 ± 0.02

3.3 Stiction Behaviors

The typical example of the friction force traces obtained from the stop-start measurement for the confined 1.4-nm PAO film is shown in Fig. 4. The confined film was slid at

a constant sliding velocity ($V = 0.11$ μm/s); kinetic friction force F_k was obtained. In the next step, sliding was stopped for a certain time t and then restarted; meanwhile, the friction force was continually measured as a function of time. When sliding was stopped, friction force dropped due to some molecular relaxation. As is shown in Fig. 4a, there was no measurable stiction spike when the surface stopping (aging) time t was 10 s. On the other hand, a stiction spike (static friction) F_s was observed at the commencement of sliding for the case of $t = 100$ s (Fig. 4b). The critical stopping time to produce stiction spike is often called a characteristic freezing time τ_f [1, 7, 22]. The stiction spike height ΔF ($= F_s - F_k$) varied with t, which will be shown in Fig. 6.

The shape of the stiction spike is different depending on the confined systems, which includes rich information on the molecular kinetic response of the systems. For the 1.4-nm PAO film, the stiction force decay (transition from F_s to F_k) shown in Fig. 4b was successfully fitted by a double exponential function and two time constants (short time constant τ_1^{PAO} and long time constant τ_2^{PAO}) were obtained. The double exponential stiction force decay was observed for the 1.4-nm PAO film under most of the experimental conditions. However, at the highest applied pressure ($P = 5.9$ MPa) and the stopping time of 1000 s, the spike force decay was fitted by a single exponential function. We should note that the time constants obtained from the fit are much longer than the mechanical time constant of the system (the order of milliseconds [23]).

Figure 5 shows the example of unique stop-start force responses observed in this study. For the confined 1.1-nm PAO film (Fig. 5a), no obvious "spike" was observed at the commencement of sliding under all the applied load and stopping time conditions. Instead, lateral force slightly larger than F_k (bump-shaped transient force) was sometimes observed. For the confined PA/PAO film, stiction force was generally larger than the confined PAO system (see Fig. 6). A very large stiction spike after long t generated a "slip overshoot" at the initial slippage process. Because of the large bent displacement of the friction-measuring spring upon large stiction spike, the immediate moving back of the spring on slipping did not stop at the equilibrium position but overshoot. Then, the spring went back to a proper (equilibrium) position (increase of the lateral force) and force relaxed again slowly with time (Fig. 5b).

Stiction spike height ΔF varies with surface stopping time t, which reflects the structural change of the intervening liquid film during stopping (aging). However, the stiction spike height also depends on the real contact area that could also change (increase) with t due to the plastic deformation of the substrate material [24, 25]. Therefore, stiction spike height normalized by the contact area ($\Delta F/A$)

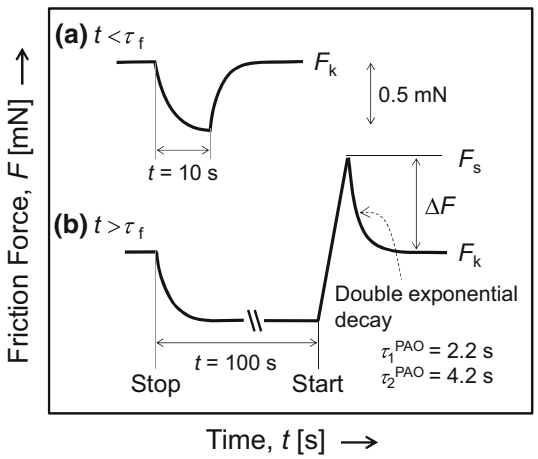

Fig. 4 Example of the stop-start measurement for the confined films of PAO ($D = 1.4$ nm). The sliding was stopped for a certain time, t, and then restarted; meanwhile, the friction force was continuously measured as a function of time. If the stopping time t was shorter than a characteristic freezing time τ_f (**a**), there was no change in the friction when sliding was restarted. However, when t exceeded τ_f (**b**), apparent stiction spike was observed. The spike force decay was fitted by a double exponential function, and two time constants (τ_1^{PAO} and τ_2^{PAO}) were obtained. Sliding conditions: $L = 30$ mN ($P = 5.2$ MPa), $V = 0.11$ μm/s

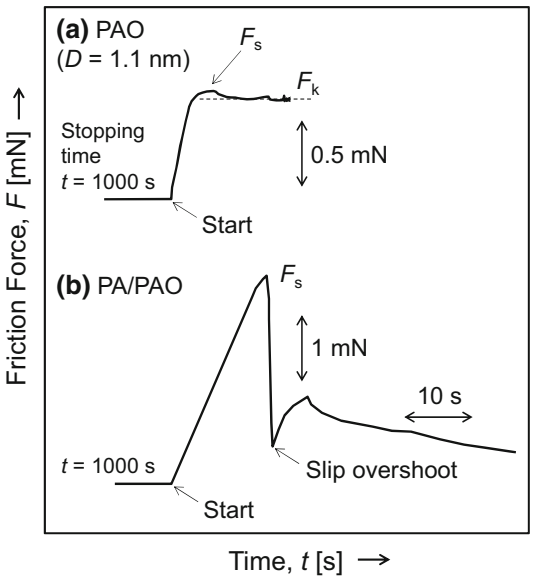

Fig. 5 Different force responses at the commencement of sliding after stopping for 1000 s for **a** confined PAO system ($D = 1.1$ nm), and **b** confined PA/PAO system. For the 1.1-nm PAO system (**a**), instead of a sharp stiction spike, we see a bump-shaped force at the commencement of sliding. For the PA/PAO system (**b**), "slip overshoot" was observed followed by a long-time force decay. Sliding conditions: **a** $L = 10$ mN ($P = 2.6$ MPa), $V = 0.11$ μm/s; and **b** $L = 15$ mN ($P = 10.4$ MPa), $V = 0.11$ μm/s

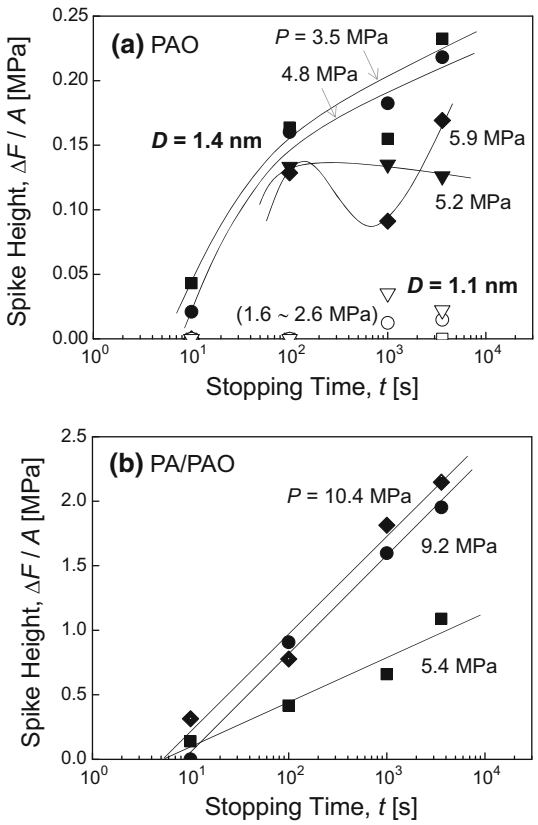

Fig. 6 Stiction spike height normalized by the contact area as a function of stopping time for the two confined systems: **a** confined PAO system; and **b** confined PA/PAO system. Because no obvious stiction spike was observed for the 1.1-nm PAO film (**a**), the height of the bump-shaped force is plotted (*open symbols*). The slip overshoot for the PA/PAO system **b** was observed when $\Delta F/A$ exceeded 1.5 MPa ($P > 9.2$ MPa and $t > 1000$ s)

was obtained as a quantitative parameter and plotted as a function of stopping time t; the results are shown in Fig. 6. For the confined PAO system (Fig. 6a), the 1.1-nm film and 1.4-nm film exhibited different stiction behaviors (as was already mentioned). The 1.1-nm film did not exhibit obvious "spike," and the height of the bump-shaped force (Fig. 5a) was plotted. This bump-shaped force was observed when t exceeded 1000 s. The 1.4-nm film exhibited a stiction spike, whose height increased with the increase of t at low P ($\leq$4.8 MPa). However, at high P conditions ($P \geq 5.2$ MPa), the $\Delta F/A$ did not exhibit a simple t dependence (data points rather scattered at $P = 5.9$ MPa). It is interesting to note that large P gave small $\Delta F/A$ at a given t. The $\Delta F/A$ of the PA/PAO film (Fig. 6b) was generally much larger than that of the PAO films. The $\Delta F/A$ increased logarithmically with t and also increase with the increase of P. Very different effects of t and P on $\Delta F/A$ between the two lubricant systems reflect different confined structures and molecular friction mechanisms, which will be discussed in the following section.

4 Discussion

4.1 Structure and Friction/Stiction of Confined PAO System

In this study, two distinct hard-wall thicknesses (1.1 ± 0.1 and 1.4 ± 0.1 nm) were obtained for the confined PAO system at different measurements. Although we cannot give a quantitative discussion, the different hard-wall thicknesses could be due to the different surface approach rates at different measurements as was already mentioned [21]. Friction coefficient μ for the 1.1-nm film was approximately 5 times larger than that of the 1.4-nm film (Fig. 3; Table 1). This difference in μ should come from the following mechanism. Figure 7a schematically illustrates the plausible structures for the two hard-wall thicknesses. Considering the molecular size of PAO, the 1.1-nm film roughly corresponds to two molecular layers (diameter of hydrocarbon chain is about 0.4 nm [1]). This means that most of the PAO molecules directly attach and adsorb onto upper or lower mica surfaces. Interdigitation between hydrocarbon chains in the molecule and molecular bridges between mica surfaces may exist, which contributes to relatively large friction [26]. On the other hand, the 1.4-nm film could have PAO molecules in the middle part of the film that do not attach to mica surfaces (shown as "non-adsorbed PAO molecule"). The non-adsorbed PAO molecules can slip between the adsorbed PAO layers, which should be the main cause of the relatively low friction of the 1.4-nm film.

The different stiction features between the two thickness films well agree to the above explanation. The 1.4-nm PAO film exhibits stiction spike after stopping (aging). This is

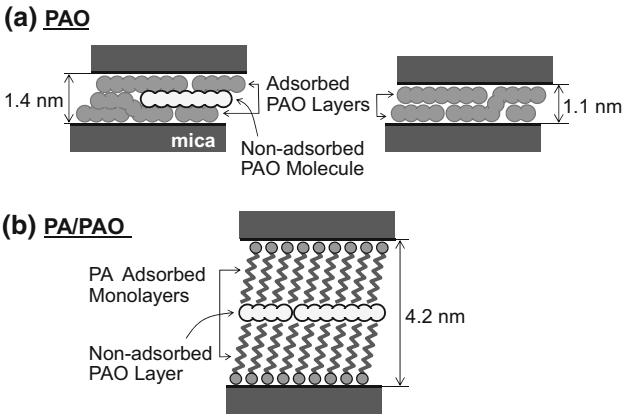

Fig. 7 Schematic illustrations of the confined film structures of the PAO and PA/PAO systems. For the PAO system (**a**), the first layers adjacent to mica substrates are strongly adsorbed on surfaces. For the 1.4-nm film, slipping is mainly accomplished by the non-adsorbed PAO molecules. For the PA/PAO system (**b**), monomolecular layer of PAO is confined between the PA adsorbed monolayers. The PAO monomolecular layer behaves as a non-adsorbed layer and exhibits a solid-like slippage over the PA monolayer surfaces

possibly due to the positional rearrangement of the non-adsorbed PAO molecules between the adsorbed PAO layers during aging that leads to a densely packed structure [7, 27]. On the other hand, the 1.1-nm film does not exhibit apparent "spike" after aging, because PAO molecules in the film are adsorbed on upper or lower mica surfaces and cannot undergo positional rearrangement into a densely packed structure. Instead, the adsorbed PAO layers undergo a viscous deformation at the commencement of sliding, which results in the bump-shaped force as is shown in Fig. 5a.

One of the authors previously studied the friction properties of the molecularly confined films of poly(dimethylsiloxane) (PDMS) between mica surfaces and observed similar behaviors [28]. The confined PDMS films had a discrete layer structure. When the thickness was larger than three molecular layers, relatively low kinetic friction and static friction were observed. On the other hand, when the thickness was decreased to two molecular layers, kinetic friction increased by a factor of 6–8 and no static friction was observed at the commencement of sliding. These friction features were interpreted by the presence or absence of non-adsorbed PDMS layer(s) in the confined films.

Now molecular mechanism of the stiction behavior of the 1.4-nm PAO film is discussed in more detail. As was already mentioned, the 1.4-nm film has non-adsorbed PAO molecules in the middle part of the film which slip between the adsorbed layers during sliding. When sliding is stopped, the structure of the film shifts from kinetic structure to static structure, which is accomplished mainly by the positional rearrangement of the non-adsorbed PAO molecules between the adsorbed layers (this results in the force drop on stopping in Fig. 4). This molecular rearrangement accompanies with the density increase (molecular volume decrease); increasing aging time leads to pack the molecules more densely. When the density in the system reaches a critical value (stopping time t reaches the critical freezing time τ_f), the whole film becomes "frozen" that generates a stiction spike (Fig. 4). Further increase of t leads the system into deeper and deeper energy minima; the stress required to bring the system out of the local energy minimum into a sliding structure ($\Delta F/A$) increases with t (Fig. 6a). This is the stiction mechanism of the 1.4-nm PAO film and referred to as "confinement-induced/aging-induced glass-like transition" [4, 6, 7, 27, 29–32]. The density increase on stopping and during aging should accompany with the thickness decrease, but we did not detect it. This is reasonable because the order of the thickness change is estimated to be less than 0.1 nm [7, 33, 34], which is below the detection limit of the FECO technique. Relatively stiff normal force spring was used in this study, which should be also the reason that we did not observe the thickness change. Increasing applied pressure P retards the timescale of molecular rearrangement and decelerates the density increase during aging; packing density at a given t decreases with P. Therefore, increasing P decreases the stiction spike height $\Delta F/A$ as is shown in Fig. 6a. Further analysis of the confined structures, please see Supplementary Material.

4.2 Structure and Friction/Stiction of Confined PA/PAO System

The hard-wall thickness of the PA/PAO system was 4.2 ± 0.1 nm, which was larger than the confined PAO system. This indicates the adsorption of PA molecules on mica surfaces from solution. Previous SFA studies suggest that the carboxylic acid group in the FA molecule tends to adsorb onto mica surfaces in organic solutions [9, 10], and the thickness of the PA monolayer adsorbed from solution was about 1.8 nm [9]. Then, the thickness of PAO confined between the PA monolayers is estimated to be 0.6 nm, which roughly corresponds to a monomolecular layer (Fig. 7b).

The hard-wall thickness of confined liquids between solid surfaces is dependent on the interaction between liquid molecules and solid surfaces. For the PAO system, the hard-wall thickness between mica surfaces obtained in this study was 1.1 nm and above. This means that non-adsorbed PAO molecules may be squeezed out during compression, but the PAO molecules adjacent to mica surfaces cannot be removed from the gap due to the adsorption onto the mica surfaces. For the PA/PAO system, the mica surfaces are covered by PA monolayers as was mentioned; PAO molecules in the gap are squeezed out during compression via slipping on the PA monolayers. In this situation, the PAO molecules adjacent to the PA monolayers should behave as non-adsorbed molecules [28]; otherwise, the PAO thickness should be larger than two molecular layers. The thickness of monomolecular layer is reached only when PAO molecules adjacent to either upper or lower PA monolayer surface are removed by compression. This discussion also implies that the hydrocarbon chains in the PAO molecule do not penetrate into the PA monolayers. As was mentioned in Introduction, Ruths et al. [9] and Lundgren et al. [10] claimed that hydrocarbon liquids (tetradecane or n-hexadecane) trapped between the adsorbed layers of saturated FAs (stearic acid or palmitic acid) penetrate into the adsorbed FA layers. This penetration induces a rather disordered structure of the confined systems that contributes to low friction. Our result implies no penetration of intervening PAO molecules into the PA monolayers for the PA/PAO system (packing density of the alkyl chain in the PA molecule is rather high in the monolayers that prevents the penetration). The penetration of liquid lubricant molecules into the adsorbed FA monolayers should be dependent on the molecular size of

the liquid; the size of PAO is larger (bulky) than that of hydrocarbon liquids. This molecular size difference could result in the different additive solubility in bulk solutions and different penetration behaviors at the liquid/adsorbed layer interface (and friction properties).

Friction force is dependent on the non-adsorbed liquid molecules in the confined system. From this viewpoint, both the PA/PAO film and 1.4-nm PAO film could have one non-adsorbed PAO layer (Fig. 7). However, friction force of the PA/PAO film is much larger than that of the 1.4-nm PAO film (Figs. 2, 3; Table 1). This is possibly due to the following reason. The structure of the 1.4-nm PAO film is not expected to be a perfect layer structure but a disordered structure; hydrocarbon chains in the PAO molecule could interdigitate between layers. This disordered conformation introduces extra molecular volume, which leads to the relatively low friction of the 1.4-nm PAO film. On the other hand, the PA/PAO film has monomolecular layer of PAO between PA monolayers and no penetration of PAO into the PA monolayers is expected, as was already discussed. The PAO molecules are highly compressed, and the packing density should be higher than the 1.4-nm PAO film, which leads to larger friction. The rigid PAO monomolecular layer between PA monolayers constitutes a solid-like "layered" interface that provides strong van der Waals adhesion, which also contributes to large friction (large F_0 in Table 1).

The observed friction behaviors well agree to the schematic model shown in Fig. 7b. The kinetic friction force decreases with the increase of sliding velocity (Fig. 2b), which indicates that the responsible friction mechanism is a solid-like slippage between the monomolecular PAO layer and PA adsorbed monolayers. This model also suits the slip overshoot shown in Fig. 5b; solid-like slippage is the initial mechanism at the commencement of sliding. Stiction spike height increases logarithmically with stopping (aging) time and increases with pressure (Fig. 6b), which is also consistent with the solid-like nature of the interface. One should note that the observed features are very different qualitatively and quantitatively from the friction between solid-like monolayers [35]. Solid-like monolayers generally exhibit stick–slip friction at low sliding velocity (typically less than 0.1 μm/s). The friction and stiction forces for such monolayers are much smaller than those observed in our PA/PAO system.

4.3 Time Constant Analysis of Stiction Spikes

The stiction spike shape shown in Figs. 4 and 5 reflects the structural transition from static state to kinetic state. As is shown in Fig. 4b, exponential fit of the decay enables us to obtain the time constants of the transition. The exponential fit is applicable not only for the confined PAO system (1.4 nm) but also for the PA/PAO system. The two time constants (short time constant τ_1 and long time constant τ_2), obtained for the spikes at the stopping time t of 1000 s, for the two confined systems are plotted as a function of applied pressure, and the results are shown in Fig. 8 (superscript for τ_1 and τ_2 represents the two confined systems). The obtained time constants are many orders of magnitude longer than bulk liquids, which indicates the retardation of molecular motions in confinement [1, 2].

As was already mentioned, the "freezing" behavior of the 1.4-nm PAO film during aging is interpreted by confinement-induced/aging-induced glass-like transition. Then, the time constants for the PAO film shown in Fig. 8 could be discussed from the Williams–Landel–Ferry (WLF) theory [36, 37] of glass-like materials (WLF theory is applicable to many different energy dissipation phenomena including friction, see [1, 31]). According to the theory, the relationship between the time constant of molecular motions τ and pressure P is described as follows:

$$\log(\tau) = C_1 + C_2 P \tag{2}$$

where C_1 and C_2 are constants [7, 27, 37]. Equation 2 was applied to the data shown in Fig. 8, and the two fitting constants (C_1 and C_2) were obtained; the results are listed in Table 2. For the PA/PAO system, $\tau_1^{PA/PAO}$ at $P = 10.4$ MPa was excluded from the fit because this data point seemed underestimate caused by the large slip overshoot at the commencement of sliding (Fig. 5b).

Equation 2 is well applicable to the results shown in Fig. 8, which supports the glass-like mechanism in the stiction dynamics. The interesting finding is that τ_2^{PAO} and $\tau_1^{PA/PAO}$ *decrease logarithmically* with P and the fitting constants (C_1 and C_2) for the two time constants are close to each other (Table 2). This excellent agreement suggests that τ_2^{PAO}

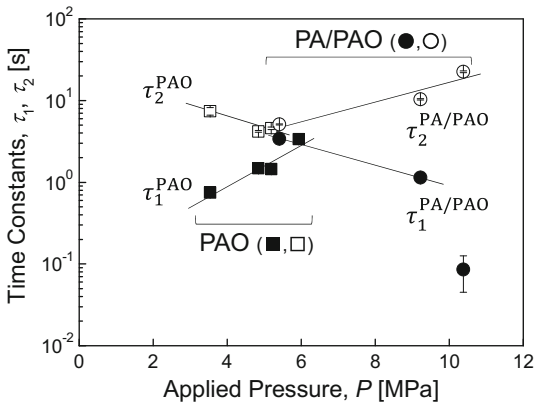

Fig. 8 Effect of applied pressure on the two time constants, short constant τ_1 (*filled symbols*) and long constant τ_2 (*open symbols*), obtained from the exponential fit of the stiction force decay of the spike at $t = 1000$ s for the confined PAO system ($D = 1.4$ nm) and the PA/PAO system. The *solid lines* represent the data fit using Eq. 2

Table 2 Fitting constants (C_1 and C_2) of the relationship between time constants of stiction force decay (short time constant τ_1 and long time constant τ_2) and applied pressure P for the results shown in Fig. 8 obtained using Eq. 2

	τ_1		τ_2	
	C_1	C_2	C_1	C_2
PAO (1.4 nm)	-1.07 ± 0.27	0.26 ± 0.05	1.37 ± 0.24	-0.14 ± 0.05
PA/PAO	1.21	−0.12	0.05 ± 0.34	0.12 ± 0.04

and $\tau_1^{PA/PAO}$ are governed by a same molecular relaxation mechanism. On the other hand, τ_1^{PAO} and $\tau_2^{PA/PAO}$ both *increase logarithmically* with P.

Now we discuss the molecular mechanisms of the two time constants. The double exponential decay of the spike force is reported by a number of authors for the stiction and stick–slip friction of confined liquids [7, 23, 27, 38, 39]. Drummond and Israelachvili discussed the mechanisms for branched hydrocarbon liquids (including PAO), which are as follows [38]: (1) local rearrangement of an individual molecule from static to kinetic conformation for the short time constant; and (2) cooperative rearrangement involving neighboring molecules for the long time constant. When we apply these assignments to our results, the two time constants for the confined PAO system are explained as follows: local rearrangement of an individual PAO molecule for τ_1^{PAO} and cooperative rearrangement involving neighboring PAO molecules for τ_2^{PAO}.

As was already discussed, the molecular mechanisms of τ_2^{PAO} and those of $\tau_1^{PA/PAO}$ should be the same deduced from the excellent agreement of the fitting constants (Table 2). Then, $\tau_1^{PA/PAO}$ should be governed by a cooperative mechanism (slippage as a monomolecular layer), which is the initial process of the stiction force decay for the PA/PAO system. Large cooperative slip at the commencement of sliding could dilate the system that introduces extra molecular volume; breaking of the cooperative structure and local rearrangements of individual molecule occur. The time constant $\tau_2^{PA/PAO}$ should be correlated with this mechanism. This discussion is consistent with the fact that the constant C_2 for both $\tau_2^{PA/PAO}$ and τ_1^{PAO} was positive (time constant of local rearrangement increases with pressure). We did not detect the dilation at the commencement of sliding for the PA/PAO system, because the dilation is expected to be less than 0.1 nm as was mentioned [7, 33, 34].

4.4 Comparison with Macroscopic Friction/Stiction Behaviors

Finally, we discuss the friction mechanism of PA additive in PAO observed by the SFA in relationship to the macroscopic friction in engineering systems. We conducted friction measurements for the contact between rough steel ball/steel disk surfaces lubricated by PAO or PA/PAO using a ball-on-disk tribometer (see Supplementary Material). The results showed that stiction spike was observed for the PAO-lubricated system, but no stiction was seen for the PA/PAO-lubricated system (Figures S1 and S2 in Supplementary Material). In addition, approximately 30 % reduction of kinetic friction was achieved by the addition of PA (Figure S3). These additive effects for macroscopic rough surfaces are compatible with previous studies [8, 9, 40–42] and are very different from our SFA results. We believe this is reasonable mainly because of the following reason. As was already discussed, the interfacial structure of PA/PAO system between mica consists of a monomolecular PAO layer confined between PA adsorbed layers, and strong van der Waals adhesion is expected between the solid-like "layered" interfaces. It is well known that FA additives in lubricant oils adsorb onto steel surface by the carboxylic group in the molecule [8]; the interfacial structure between mica surfaces (Fig. 7b) should be not very different from the structure at the each contact asperity between rough steel/steel surfaces. Then, large kinetic friction/stiction for the smooth contact (SFA) and low kinetic friction/stiction for the macroscopic rough contacts could be due to the different fraction of real contact area. Surface roughness extensively reduces the real contact area that weakens van der Waals adhesion and friction of the solid-like interface. This is basically the same as the common observations in adhesion measurements at the molecular and macroscopic scales; solid/solid contact interface at the molecular scale (single-asperity contact) is generally adhesive, whereas most of the macroscopic contact interface is not sticky (referred to as "adhesion paradox") [43–45]. On the other hand, the kinetic friction and stiction for the PAO system between smooth mica surfaces are determined by the extreme increase in the viscosity (and resulting glass-like transition) of PAO in confinement. This viscosity increase is also expected at the each contact asperity between rough steel surfaces lubricated by PAO; this is probably the reason that macroscopic steel surfaces lubricated by PAO exhibit relatively large kinetic friction (than additive system) and generate stiction. Our results suggest that the advantage of

saturated FA additives in the oil-based lubrication of mechanical engineering systems comes from the solid-like nature of the contact interfaces provided by the FA monolayers adsorbed on surfaces.

5 Conclusions

The kinetic friction and stiction properties of the dilute solution of palmitic acid (PA) in poly(α-olefin) (PAO) confined between molecularly smooth mica surfaces were investigated using the SFA. The hard-wall thickness of the PA/PAO system was 4.2 ± 0.1 nm, which corresponds to a monomolecular layer of PAO confined between PA adsorbed monolayers on opposed mica surfaces. The kinetic friction and stiction are governed by the solid-like slippage of PAO monomolecular layer between the PA adsorbed monolayer; our results imply no penetration of PAO molecules into the PA monolayers (adsorbed PA molecules form rather rigid monolayers). Highly compressed/confined PAO monomolecular layer between the PA monolayers constitutes a solid-like "layered" interface, which produces large van der Waals adhesion and large friction/stiction for molecularly smooth contact interface. However, the solid-like interfacial nature induced by the PA additive offers the advantage of reducing kinetic friction and stiction for macroscopic rough surfaces, because surface roughness extensively reduces the real contact area and thus weakens van der Waals adhesion and friction of solid-like contact interface.

Acknowledgments The authors thank S. Yoshida for her experimental assistance. This work was supported by "Tohoku Innovative Materials Technology Initiatives for Reconstruction (TIMT)" funded by the Ministry of Education, Culture, Sports, Science and Technology (MEXT) and Reconstruction Agency, Japan. S.Y. thanks Kao Corporation for their support.

Compliance with Ethical Standards

Conflict of interest The authors declare that they have no conflict of interest.

References

1. Israelachvili, J.N.: Intermolecular and Surface Forces, 3rd edn. Academic Press, Amsterdam (2011)
2. Israelachvili, J., Berman, A.D.: Surface forces and microrheology of molecularly thin liquid films. In: Bhushan, B. (ed.) CRC Handbook of Micro/Nanotribology, 2nd edn, pp. 371–432. CRC Press, Boca Raton (1999)
3. Granick, S.: Motions and relaxations of confined liquids. Science **253**, 1374–1379 (1991)
4. Robbins, M.O., Müser, M.H.: Computer simulations of friction, lubrication and wear. In: Bhushan, B. (ed.) Modern Tribology Handbook, vol. One, pp. 717–765. CRC Press, Boca Raton (2001)
5. Watanabe, J., Mizukami, M., Kurihara, K.: Resonance shear measurement of confined alkylphenyl ether lubricants. Tribol. Lett. **56**, 501–508 (2014)
6. Yamada, S.: General shear-thinning dynamics of confined fluids. Tribol. Lett. **13**, 167–171 (2002)
7. Yamada, S.: Structural aging and stiction dynamics in confined liquid films. J. Chem. Phys. **131**, 184708 (2009)
8. Spikes, H.: Friction modifier additives. Tribol. Lett. **60**, 5 (2015)
9. Ruths, M., Ohtani, H., Greenfield, M., Granick, S.: Exploring the "friction modifier" phenomenon: nanorheology of *n*-alkane chains with polar terminus dissolved in *n*-alkane solvent. Tribol. Lett. **6**, 207–214 (1999)
10. Lundgren, S.M., Ruths, M., Danerlöv, K., Persson, K.: Effects of unsaturation on film structure and friction of fatty acids in a model base oil. J. Colloid Interface Sci. **326**, 530–536 (2008)
11. Doig, M., Warrens, C.P., Camp, P.J.: Structure and friction of stearic acid and oleic acid films adsorbed on iron oxide surfaces in squalane. Langmuir **30**, 186–195 (2014)
12. Martin, J.M., Matta, C., Bouchet, M.-I.D.B., Forest, C., Monge, T.L., Dubois, T., Mazarin, M.: Mechanism of friction reduction of unsaturated fatty acids as additives in diesel fuels. Friction **1**, 252–258 (2013)
13. Israelachvili, J., Min, Y., Akbulut, M., Alig, A., Carver, G., Greene, W., Kristiansen, K., Meyer, E., Pesika, N., Rosenberg, K., Zeng, H.: Recent advances in the surface forces apparatus (SFA) technique. Rep. Prog. Phys. **73**, 036601 (2010)
14. Ren, H.Y., Mizukami, M., Tanabe, T., Furukawa, H., Kurihara, K.: Friction of polymer hydrogels studied by resonance shear measurements. Soft Matter **11**, 6192–6200 (2015)
15. Lakes, S.C.: Automotive Gear Lubricants. In: Rudnick, L.R. (ed.) Synthetics, mineral oils, and bio-based lubricants: chemistry and technology, 2nd edn, pp. 459–472. CRC Press, Taylor and Francis Group, Boca Raton (2013)
16. Kawai, H., Sakuma, H., Mizukami, M., Abe, T., Fukao, Y., Tajima, H., Kurihara, K.: New surface forces apparatus using two-beam interferometry. Rev. Sci. Instrum. **79**, 043701 (2008)
17. Luengo, G., Schmitt, F.J., Hill, R., Israelachvili, J.: Thin film rheology and tribology of confined polymer melts: contrast with bulk properties. Macromolecules **30**, 2482–2494 (1997)
18. Dushkin, C.D., Kurihara, K.: Nanotribology of thin liquid-crystal films studied by the shear force resonance method. Colloids Surf. A **129–130**, 131–139 (1997)
19. Israelachvili, J.: Thin film studies using multiple-beam interferometry. J. Colloid Interface Sci. **44**, 259–272 (1973)
20. Yamada, S., Fujihara, A., Yusa, S., Tanabe, T., Kurihara, K.: Low-friction adsorbed layers of a triblock copolymer additive in oil-based lubrication. Langmuir **31**, 12140–12147 (2015)
21. Bureau, L.: Rate effects on layering of a confined linear alkane. Phys. Rev. Lett. **99**, 225503 (2007)
22. Yoshizawa, H., Israelachvili, J.: Fundamental mechanisms of interfacial friction. 2. Stick-slip friction of spherical and chain molecules. J. Phys. Chem. **97**, 11300–11313 (1993)
23. Drummond, C., Israelachvili, J.: Dynamic phase transitions in confined lubricant fluids under shear. Phys. Rev. E **63**, 041506 (2001)

24. Caroli, C., Baumberger, T., Bureau, L.: Static aging vs. dynamic rejuvenation in solid friction. J. Phys. IV Fr. **12**(Pr9), 269–273 (2002)
25. Bureau, L., Baumberger, T., Caroli, C.: Rheological aging and rejuvenation in solid friction contacts. Eur. Phys. J. E **8**, 331–337 (2002)
26. Raviv, U., Tadmor, R., Klein, J.: Shear and frictional interactions between adsorbed polymer layers in a good solvent. J. Phys. Chem. B **105**, 8125–8134 (2001)
27. Yamada, S.: Aging and stiction dynamics in confined films of a star polymer melt. J. Chem. Phys. **137**, 194702 (2012)
28. Yamada, S.: Layering transitions and tribology of molecularly thin films of poly(dimethylsiloxane). Langmuir **19**, 7399–7405 (2003)
29. Robbins, M.O., Baljon, A.R.C.: Response of thin oligomer films to steady and transient shear. In: Tsukruk, V.V., Wahl, K.J. (eds.) Microstructure and Microtribology of Polymer Surfaces, ACS Symposium Series vol. 741. Chapter 6, pp. 91–115. American Chemical Society, Washington, DC (2000)
30. Hu, H.W., Carson, G.A., Granick, S.: Relaxation time of confined liquids under shear. Phys. Rev. Lett. **66**, 2758–2761 (1991)
31. Demirel, A.L., Granick, S.: Glasslike transition of a confined simple fluid. Phys. Rev. Lett. **77**, 2261–2264 (1996)
32. Yamada, S., Nakamura, G., Hanada, Y., Amiya, T.: Glasslike transitions in thin polymer-melt films due to thickness constraint. Tribol. Lett. **15**, 83–89 (2003)
33. Dhinojwala, A., Bae, S.C., Granick, S.: Shear-induced dilation of confined liquid films. Tribol. Lett. **9**, 55–62 (2000)
34. Demirel, A.L., Granick, S.: Lubricated friction and volume dilatancy are coupled. J. Chem. Phys. **117**, 7745–7750 (2002)
35. Yoshizawa, H., Chen, Y.L., Israelachvili, J.: Fundamental mechanisms of interfacial friction. 1. Relation between adhesion and friction. J. Phys. Chem. **97**, 4128–4140 (1993)
36. Ferry, J.D.: Viscoelastic Properties Of Polymers, 3rd edn. Wiley, New York (1980)
37. Sperling, L.H.: Introduction to Physical Polymer Science, 3rd edn. Wiley Interscience, New Yolk (2001)
38. Drummond, C., Israelachvili, J.: Dynamic behavior of confined branched hydrocarbon lubricant fluids under shear. Macromolecules **33**, 4910–4920 (2000)
39. Berman, A.D., Ducker, W.A., Israelachvili, J.N.: Origin and characterization of different stick–slip friction mechanisms. Langmuir **12**, 4559–4563 (1996)
40. Rounds, F.G.: Effect of lubricant composition on friction as measured with thrust ball bearings. J. Chem. Eng. Data **5**, 499–507 (1960)
41. Zhu, Y., Ohtani, H., Greenfield, M.L., Ruths, M., Granick, S.: Modification of boundary lubrication by oil-soluble friction modifier additives. Tribol. Lett. **15**, 127–134 (2003)
42. Smith, O., Priest, M., Taylor, R.I., Price, R., Cantlay, A., Coy, R.C.: Simulated fuel dilution and friction-modifier effects on piston ring friction. Proc. Inst. Mech. Eng. J J. Eng. Tribol. **220**, 181–189 (2006)
43. Pastewka, L., Robbins, M.O.: Contact between rough surfaces and a criterion for macroscopic adhesion. Proc. Natl. Acad. Sci. USA **111**, 3298–3303 (2014)
44. Kendall, K.: Molecular Adhesion and Its Application: The Sticky Universe. Kluwer Academic, New York (2001)
45. Zappone, B., Rosenberg, K.J., Israelachvili, J.: Role of nanometer roughness on the adhesion and friction of a rough polymer surface and a molecularly smooth mica surface. Tribol. Lett. **26**, 191–201 (2007)